$S = \frac{1}{2}$ kagome Heisenberg antiferromagnet revisited

Andreas M. Läuchli,[1] Julien Sudan,[2] and Roderich Moessner[3]
[1]*Institut für Theoretische Physik, Universität Innsbruck, A-6020 Innsbruck, Austria*
[2]*Rue du Stand 16, CH-2053 Cernier, Switzerland*
[3]*Max-Planck-Institut für Physik komplexer Systeme, Nöthnitzer Straße 38, D-01187 Dresden, Germany*

(Received 5 December 2016; revised manuscript received 7 October 2019; published 28 October 2019)

We examine the perennial quantum spin liquid candidate $S = \frac{1}{2}$ Heisenberg antiferromagnet on the kagome lattice. Our paper is based on achieving Lanczos diagonalization of the Hamiltonian on a 48 site cluster in sectors with dimensions as large as 5×10^{11}. The results reveal intricate structures in the low-lying energy spectrum. These structures by no means unambiguously support a $\mathbb{Z}_2$ spin liquid ground state, but instead appear compatible with several scenarios, including fourfold topological degeneracy, inversion symmetry breaking, and a combination thereof. We discuss finite-size effects, such as the apparent absence of the eigenstate thermalization hypothesis, and note that, while considerably reduced, some are still present for the largest cluster. Finally, we observe that an XXZ model in the Ising limit reproduces remarkably well the most striking features of finite-size spectra.

DOI: 10.1103/PhysRevB.100.155142

I. INTRODUCTION

The $S = \frac{1}{2}$ kagome Heisenberg magnet is arguably the best studied, yet most enigmatic, candidate spin liquid, identified as such in the very early works of the field of highly frustrated magnetism [1,2]. Many different numerical approaches have been applied to this magnet: exact diagonalization (ED) [1–10], resonating valence bond (RVB) physics inspired methods [11–19], variational Monte Carlo [20–25], coupled cluster treatments [26], contractor renormalization (CORE) [27–29], series expansions [30,31], density-matrix renormalization group (DMRG) [32–37], and tensor network algorithms [38–42].

These have yielded an enigmatic phenomenology, with evidence for the following features: (a) all correlations are short ranged; (b) the singlet gap, if nonvanishing, is numerically tiny; (c) there exists a huge number of (near-)degenerate states apparently not related by symmetry; (d) these spectral features are remarkably stable for classes of perturbations around the Heisenberg point. On general grounds, it is not clear how to reconcile these, in particular (a) with (b), and (c) with (d).

Given these confusing signals, it is perhaps not surprising that confidence in various pictures of the behavior of this magnet has ebbed and flowed, with new technologies providing invaluable new insights which in turn generate new scenarios of varying shelf life. An important breakthrough was a DMRG tour de force by Yan and coworkers [33] and a number of follow-up studies using that method [34,35], as it turns into a tool for the study of two-dimensional magnets. Taken together, these suggested as the most likely scenario a $\mathbb{Z}_2$ gapped spin liquid, based on the observation that correlations appear to be short ranged, with candidate ordering patterns imposed at the boundaries decaying swiftly into the bulk. Evaluations of the universal contribution to the entanglement entropy show, with differing degrees of confidence, the value expected for this topological state [34,35].

A source of uncertainty hard to quantify in this evidence lies in the fact that DMRG is not an unbiased method, preferring low-entanglement states over highly entangled ones, so that the last word may very well not have been spoken. Indeed, a more recent DMRG study employing flux threading found evidence for a much smaller spin gap than that given by previous DMRG estimates, and suggested the possibility of a U(1) spin liquid with an excitation spectrum containing (gapless) Dirac cones [37].

Against this background, the work reported here revisits possible alternative scenarios. The material presented here is based on state-of-the-art exact diagonalization work. This is in the tradition of exact diagonalization studies that have historically been a linchpin of the study of kagome; their main advantage is that they are numerically exact and unbiased, while providing a comprehensive picture of the low-energy physics, including the quantum numbers of the excitation spectrum above the ground state. The main disadvantage lies in the limitation to finite sizes, which even given Moore's law is only being pushed back slowly.

The quantifiable technical advance lies in our capacity to treat a cluster of 48 sites with a Hilbert-space dimension of $2^{48} \approx 2.8 \times 10^{14}$. Using a highly optimized, message-passing based ED code it has been possible to obtain the low-lying energy spectrum in symmetry sectors comprising up to $\approx 5 \times 10^{11}$ states. To the best of our knowledge, this is among the largest number of $S = \frac{1}{2}$ spins treated in exact diagonalization in a comparable context.

Physically, the 48 site cluster has the following important properties. First, it is a highly symmetric cluster. Second, it is compatible with many of the principal proposed ordering patterns. And, third, it severely reduces finite-size effects by eliminating a large class of winding loops (loops on the lattice winding around the periodic boundary) of length $L = 8$ present for the hitherto largest-studied 36 and 42 site clusters [43].

In the following, we first report the data on energies and gaps, which can act as benchmark and reference for the future. For the 48 site cluster, the ED ground-state energy is comfortably below that determined from DMRG. Next, we discuss the structure of the low-lying energy spectrum, which turns out to be consistent with inversion symmetry breaking, or with the presence of a topological degeneracy. We provide a detailed analysis of correlations for a large system, both spin-spin and energy-energy (dimer-dimer) correlators. We discuss different finite-size effects, most importantly an apparent absence of eigenstate thermalization, and structural shifts of levels with respect to each other. Finally, we identify the XXZ antiferromagnet in the Ising limit, $J_{xy} = 1$, $\Delta \to \infty$ (or equivalently $j \equiv J_{xy}/J_z \ll 1$), with its considerably reduced Hilbert space, as an effective model for the low-energy sector of the Heisenberg magnet, thereby extending the stability of its behavior to the full range of quantum models $0 < j \leqslant \infty$ [44,45]. We conclude with a discussion.

II. MODEL AND METHOD

We investigate the $S = \frac{1}{2}$ antiferromagnetic Heisenberg model on the kagome lattice

$$H = J \sum_{\langle i,j \rangle} \mathbf{S}_i \cdot \mathbf{S}_j, \tag{1}$$

with the coupling constant set to $J = 1$. We investigate the low-lying energy spectrum of finite kagome clusters with periodic boundary conditions with $N_s = 36$, 42, and 48 sites [46]. We apply a recently developed massively parallel exact diagonalization code to study these systems, tackling Hilbert spaces of up to 5×10^{11} basis states. Convergence within a few hundred iterations is typically reached for the lowest two to three eigenstates in each symmetry sector.

Energy spectroscopy is a powerful technique to diagnose various states of quantum matter. A characteristic "Tower of States" accompanies continuous and discrete symmetry breaking, the effective theory describing quantum critical points in one and two dimensions [47] can be accessed this way, and ground-state degeneracy of topological origin is also directly visible.

Given the earlier DMRG evidence for $\mathbb{Z}_2$ topological order in the kagome antiferromagnet, it thus appears highly desirable to evidence the required fourfold ground-state degeneracy in ED as well. In the recent activity on chiral spin liquids [48–51] it has been possible to observe the twofold (or fourfold) ground-state degeneracy even with modest system sizes accessible by ED, while DMRG simulations for the kagome Heisenberg antiferromagnet have failed to report the required ground-state degeneracy so far. In one of the simplest RVB states on the kagome lattice originating from the quantum dimer model of Misguich *et al.* [14], we would expect two lying levels each at the Γ and the (unique) M point for $N_s = 42$, while four levels at the Γ point are expected for $N_s = 36$ and 48 [52]

III. $N_s = 42$ SITE SPECTRUM

Let us first discuss the symmetry sector resolved low-energy spectrum of the $N_s = 42$ site cluster. The ground-state energy and spin gap of this cluster have been reported previously [7,8], but not the momentum and lattice π-rotation resolved low-energy spectrum. We display the spectrum in panel (a) of Fig. 1. For comparison we show the classic [6] low-energy spectrum of the highly symmetric $N_s = 36$ site sample in panel (b) on the same scale.

The kagome antiferromagnet is notorious for its rather dense low-energy spectrum [5,6,12]. In the $N_s = 36$ sample there is a subspace (including degeneracy) of about 200 singlets below the first triplet in the spectrum, with the singlet singlet gap about $0.01011J$. Despite not being able to fully converge all the singlets before the first triplet in the $N_s = 42$ case, it is nevertheless apparent that the low-energy spectrum is still very dense. Taking the number of all the approximate eigenvalues below the triplet gap as a lower bound for the exact number of singlets, we obtain at least 160 states. The singlet-singlet gap is $0.01974J$, which remarkably is almost two times larger than for $N_s = 36$. Furthermore no obvious separation of a low-lying set of multiplets forming the ground space and the rest of the spectrum is visible.

IV. $N_s = 48$ SITE SPECTRUM

To break down the full Hilbert space into manageable sectors, we use total S^z conservation, spin-flip symmetry, translation, and point-group symmetries in order, obtaining tractable subspaces of dimension up to $\approx 5 \times 10^{11}$. It is currently not possible to simultaneously exploit the complete SU(2) symmetry group *and* the lattice space group in large-scale exact diagonalizations. For performance reasons we only use a subset of the full D_6 point group, generated by the π rotation around the center of a hexagon, as well as a reflection along either the x or y axis, depending on the momentum sector under consideration. When labeling spatial symmetry sectors we state the momentum sector, followed by the eigenvalue $+1$(e) or -1(o) of the π rotation and/or the reflection. Using this smaller symmetry group it is nevertheless possible to identify the representation of D_6 by a compatibility table of the representations of the two symmetry groups. We have been able to obtain the lowest energy in all $S^z = 0$ sectors with even spin-parity and all but four in the odd spin-parity sectors. The available energies are listed in Table I in Appendix A. The ground-state energy of the 48 site cluster is $E/NJ = -0.438\ 703\ 897\ 156$, almost 0.5% lower than some of the previous DMRG studies for the same cluster [32,34]. Based on the available triplet sectors our estimate for the spin gap is $\Delta_{S=1}/J = 0.168\ 217$, while the singlet-singlet gap is $\Delta_{S=0}/J = 0.021\ 217$. The spin gap is comparable to earlier CORE [28] and variational results [25] on the same system size [53].

The low-energy spectrum of the 48 site cluster is shown in Fig. 2. In an ideal $\mathbb{Z}_2$ spin liquid situation with a short correlation length one would expect an approximate, but clear-cut, fourfold ground-state degeneracy, with a gap to all further excitations. This is not what we observe here, implying that the spin liquid state of the kagome Heisenberg antiferromagnet is either a $\mathbb{Z}_2$ spin liquid, but with significantly larger correlation lengths than anticipated based on the previous DMRG studies, or we are observing a more complex spin liquid state. While

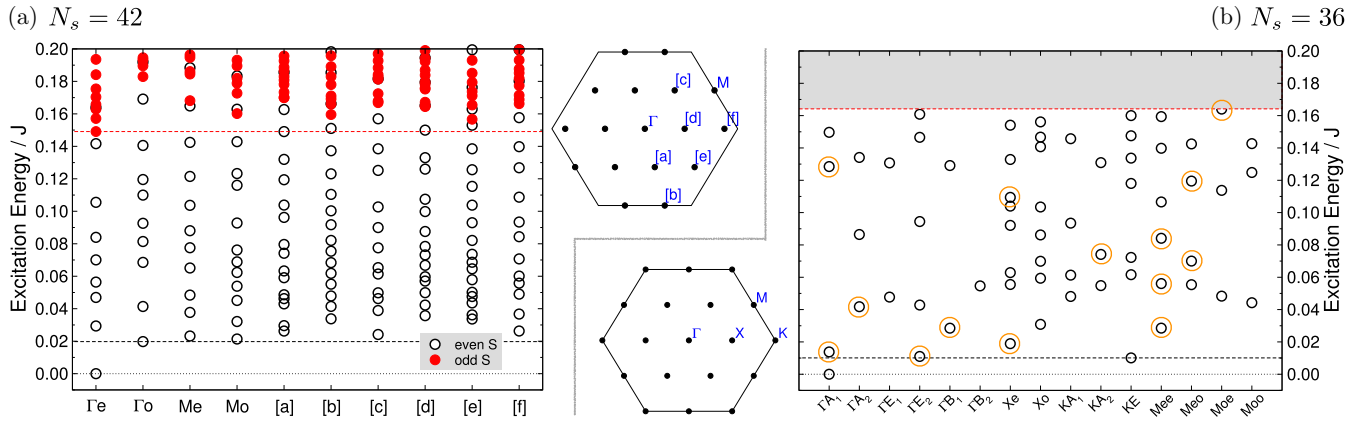

FIG. 1. Low-energy Lanczos spectra of the $S = \frac{1}{2}$ Heisenberg model for clusters with (a) $N_s = 42$ and (b) $N_s = 36$ sites. The black, empty symbols denote singlet levels, while the the red, full symbols indicate triplet levels. The black and red dashed lines indicate the location of the singlet-singlet and singlet-triplet gap. The spectrum for $N_s = 42$ is only totally converged for the lowest level in each symmetry sector. We nevertheless plot the complete spectrum of the tridiagonal Lanczos matrix in order to provide a visual impression of the buildup of a comparatively high density of states in the low-energy spectrum. The spectrum shown for $N_s = 36$ is fully converged. In the center we display the Brillouin zones of the two clusters including the labeling of the discrete k points. The additional orange circles in (b) denote eigenstates with pronounced dimer-dimer correlations (see main text for details).

we are not able to pinpoint which scenario is realized based on the available system sizes, there nevertheless are a few pointers for the largest system size. In Fig. 2 we have labeled the four expected energy levels for one of the $\mathbb{Z}_2$ spin liquids with the labels (1),(2) [an exact doublet], and (3), all of them at the Γ point in the Brillouin zone. Curiously the first excited state is not part of this set of levels, but seems to be part of an energy-shifted "shadow" structure of levels (*i*) to (*iii*) which differs from (1) to (3) in their odd quantum number with respect to π lattice rotations. It is also worth pointing out that the lowest singlet excitations at *finite* momentum,

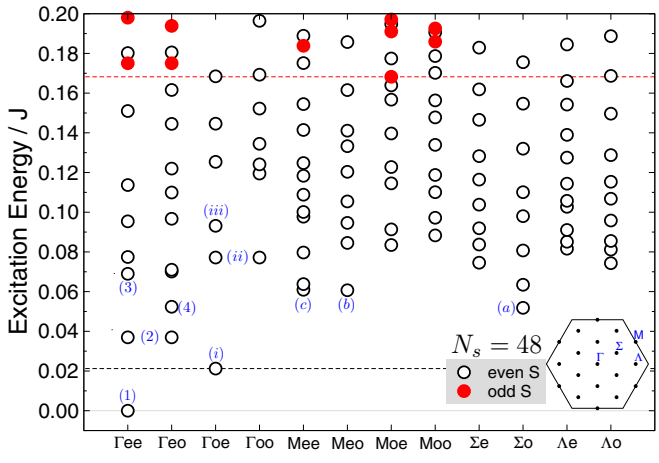

FIG. 2. Low-energy Lanczos spectrum of the $S = \frac{1}{2}$ Heisenberg model for a cluster with $N_s = 48$ sites. Black and red dashed lines indicate the location of the singlet-singlet and singlet-triplet gap. The spectrum is only completely converged for the lowest level in each symmetry sector. We nevertheless plot the complete spectrum of the final tridiagonal Lanczos matrix in order to provide an approximate visual impression of the low-energy spectrum. Labeled energy levels are discussed in the main text.

e.g., levels (a)–(c), are at comparatively high energies of $\approx 0.05J$ and above. This is in stark contrast to the 36 and 42 site samples, where the lowest finite momentum levels are either the first excited levels overall or very close in energy (see Fig. 1).

V. $N_s = 48$ SITE CORRELATION FUNCTIONS

In order to explore whether the lowest excited state—located in the Γ_{oe} sector—is related to a rotation symmetry-breaking tendency, we have calculated selected correlation functions in the ground state and the first level in the Γ_{oe} sector. Figure 3(a) displays $\langle S_0^z S_i^z \rangle$ in the ground state. As in previous work [7], we find that the strongest spin-spin correlations are not around the hexagon to which the reference site belongs, but instead along the path which connects the reference site with its image under periodic boundary conditions (indicated by the straight dashed line). Another interesting structure is the (weak) staggered correlation signal along a *diamond* path (indicated by a dashed diamond lozenge). The correlations in the first excited state are not shown, but are also weak apart from the wrapping path. In Figs. 3(b) and 3(c) we display the connected "$S^z S^z$-dimer" correlations: $\mathcal{C}^{zzzz}(i,j,k,l) = \langle (S_i^z S_j^z)(S_k^z S_l^z) \rangle - \langle (S_i^z S_j^z) \rangle \langle (S_k^z S_l^z) \rangle$, where (i,j) and (k,l) denote nearest-neighbor bonds. These are diagonal in the computational basis and therefore computationally friendlier for the large Hilbert spaces under consideration. In the ground state [panel (b)] the correlations show some interesting structure at short and intermediate distances. We observe a correlation sign pattern which is largely in agreement with a diamond valence bond crystal, first discussed in the DMRG study [33], and more recently found to be a stable phase in an extended Heisenberg model including ferromagnetic further neighbor couplings [10]. The first excited state in the sector Γ_{oe} [panel (c)] also exhibits sizable correlations, with the signs of many

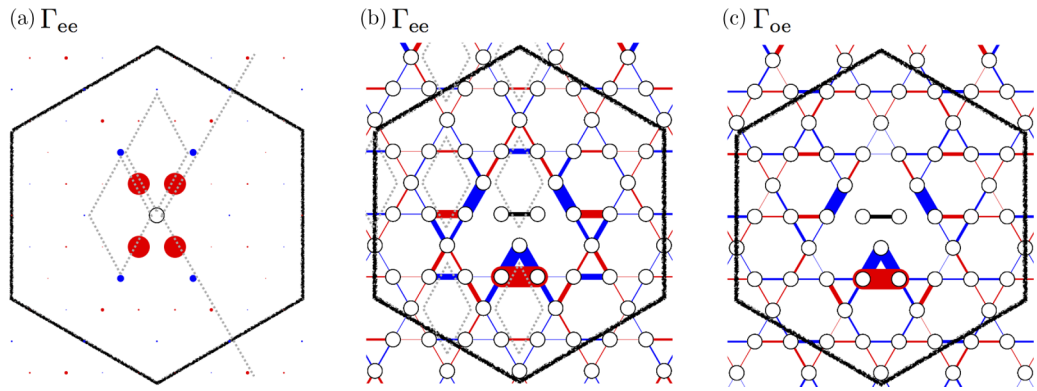

FIG. 3. Selected correlators for the 48 site cluster. Filled red (blue) objects denote negative (positive) correlations. Diameters are proportional to correlation strength. (a) $\langle S_0^z S_i^z \rangle$ correlations in the ground state. The empty circle denotes the reference site. (b) Connected $\langle (S_i^z S_j^z)(S_k^z S_l^z) \rangle - \langle (S_i^z S_j^z) \rangle \langle (S_k^z S_l^z) \rangle$ nearest-neighbor "dimer" correlations in the ground state. The black bond denotes the reference bond. (c) Connected "dimer" correlations in the first excited state (Γ_{oe} sector).

correlators changed compared to the ground state. We thus do not find evidence for a valence bond type of symmetry breaking tendency.

VI. LOW-LYING SINGLET LEVELS

The large number of low-lying singlets is a hallmark feature in ED studies of the kagome Heisenberg antiferromagnet. Despite the long history of the problem, the nature of the singlets and a *quantitative* effective Hamiltonian describing their energetics have been elusive. Here we provide a perspective on these questions. First we have determined the nearest-neighbor dimer-dimer correlations in all the singlet eigenstates of the $N_s = 36$ site cluster below the spin gap. In Fig. 1(b) we highlight those levels with an orange circle which exhibits particularly strong dimer-dimer correlations (presented in detail in Fig. 5 in Appendix B). The fact that these are broadly scattered across the investigated energy range is a strong indication that the eigenstate thermalization hypothesis (ETH) [54] is not (yet) operative. While this is not unexpected at the boundaries of a many-body spectrum, it is puzzling nevertheless, since the level spacing is already quite small, reminiscent of the situation in the inner part of a many-body energy spectrum.

VII. EFFECTIVE HAMILTONIAN

In a recent work two of us have uncovered a striking stability of the energy spectrum of the Heisenberg antiferromagnet as one moves towards the easy-plane XY limit [44]. Furthermore there is also a remarkable continuity towards the Ising limit perturbed with in-plane exchange, as observed in ground-state properties of DMRG simulations [45]. This limit has the interesting property that the effective Hilbert space is reduced, because only the antiferromagnetic Ising ground states of the kagome lattice need to be retained. For the 48 site cluster this amounts to a reduction by a factor of ≈1000 in total Hilbert-space size. In Fig. 4 we present the energy spectrum of the XY-exchange perturbed antiferromagnetic Ising model to first order in degenerate perturbation theory for the 48 site cluster. Interestingly many features of the Heisenberg singlet spectrum of Fig. 2 can be found here as well. For example, the approximate multiplets (1)–(3) and (i)–(iii) are found at similar locations in the spectrum. Furthermore the lowest finite-momentum excitations (a) and (c) are also low in energy in the effective model. However, there are also some differences, for example, the level (4) [(b)] is pushed down [up] somewhat when going from the Heisenberg spectrum to the effective XXZ model. Overall we feel that the XY-perturbed antiferromagnetic Ising configurations on the kagome lattice yield a useful effective Hamiltonian, which is actually able to reproduce many features of the low-energy spectrum of the Heisenberg antiferromagnet, and which might be pushed to larger system sizes, thereby possibly revealing the true nature of the ground state of the kagome Heisenberg antiferromagnet.

VIII. CONCLUSIONS

Even for the highly symmetric large $N_s = 48$ site cluster, no clear $\mathbb{Z}_2$ spin liquid evidence emerges. Also, correlations and spectra at finite wave vectors do not suggest valence bond ordering. Absent a quantitative understanding of how a U(1)

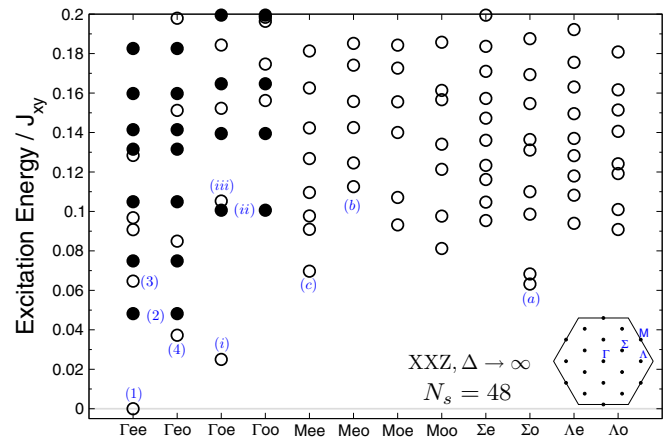

FIG. 4. XY perturbed antiferromagnetic Ising model (large Δ XXZ limit) of the $N_s = 48$ site kagome system.

spin liquid and its Dirac cones would show up in the finite-size spectrum on a torus, we cannot judge the likely validity of this scenario [37]. While finite-size effects are clearly still present in our results, some features nonetheless demand special attention. For instance, one might have expected the gross features of the physics in the ground state to prevail among the lowest excited states, as it is the case for ordered magnets or valence bond crystals. The absence of ETH in the dimer-dimer correlations then rather suggests that the low-lying singlets of the kagome antiferromagnet are not just a "soup" of featureless singlets, but instead seem to host a large number of possibly competing many-body states. In such a setting, even mildly suboptimal energies obtained variationally may reflect correlations in the trial state a long way from those of the true ground state—e.g., an error of only 0.5% in the ground-state energy of a 48 site cluster amounts to several times its singlet-singlet gap, a region which hosts quite a number of many-body levels. These aspects clearly require further study. With ongoing progress on several fronts—numerically (not least DMRG and ED), field theoretically, and with effective models—the emergence of a consistent picture may perhaps not prove to be quite so elusive in the foreseeable future.

ACKNOWLEDGMENTS

We are grateful to Yin-chen He, Frank Pollmann, and Alexander Wietek for various discussions, and acknowledge the generous support by the Max Planck Computing Centre in Garching. The simulations were performed on the BlueGene/P and on the PKS-AIMS cluster at the MPG RZ Garching, as well as on the MACH SGI Altix UV machine operated by Uni Innsbruck and Uni Linz. A.M.L. acknowledges support by the Austrian Science Fund (FWF) through Grant No. DFG-FOR1807 (I-2868) and the SFB FoQus (F-4018). R.M. acknowledges Deutsche Forschungsgemeinschaft support via Grant No. SFB 1143.

TABLE I. Lowest energy in each spatial and spin rotation symmetry sector considered for the $N_s = 48$ site kagome Heisenberg cluster.

Momentum	R_π	σ_x (σ_y)	S_{total}	E/J
Γ	$+1$	$+1$	Even	$-21.057\,787\,063$
Γ	$+1$	-1	Even	$-21.020\,818\,760$
Γ	-1	$+1$	Even	$-21.036\,569\,782$
Γ	-1	-1	Even	$-20.980\,603\,362$
M	$+1$	$+1$	Even	$-20.996\,851\,415$
M	$+1$	-1	Even	$-20.997\,096\,022$
M	-1	$+1$	Even	$-20.974\,317\,519$
M	-1	-1	Even	$-20.969\,472\,027$
Σ	$\times$	$+1$	Even	$-20.983\,214$
Σ	$\times$	-1	Even	$-21.005\,970$
Λ	$\times$	$+1$	Even	$-20.976\,185$
Λ	$\times$	-1	Even	$-20.983\,468$
Γ	$+1$	$+1$	Odd	$-20.882\,732\,807$
Γ	$+1$	-1	Odd	$-20.882\,732\,807$
Γ	-1	$+1$	Odd	$-20.856\,149\,771$
Γ	-1	-1	Odd	$-20.854\,596\,491$
M	$+1$	$+1$	Odd	$-20.873\,944\,088$
M	$+1$	-1	Odd	$-20.848\,993\,609$
M	-1	$+1$	Odd	$-20.889\,569\,935$
M	-1	-1	Odd	$-20.871\,871\,569$
Σ	$\times$	$+1$	Odd	N/A
Σ	$\times$	-1	Odd	N/A
Λ	$\times$	$+1$	Odd	N/A
Λ	$\times$	-1	Odd	N/A

APPENDIX A: ENERGY SPECTRUM FOR $N_s = 48$

In Table I we list the lowest energy in each of the targeted sectors for future reference.

APPENDIX B: DIMER-DIMER CORRELATION FUNCTIONS IN SELECTED EIGENSTATES FOR $N_s = 36$

In Fig. 5 we show dimer-dimer correlation functions in selected eigenstates for $N_s = 36$.

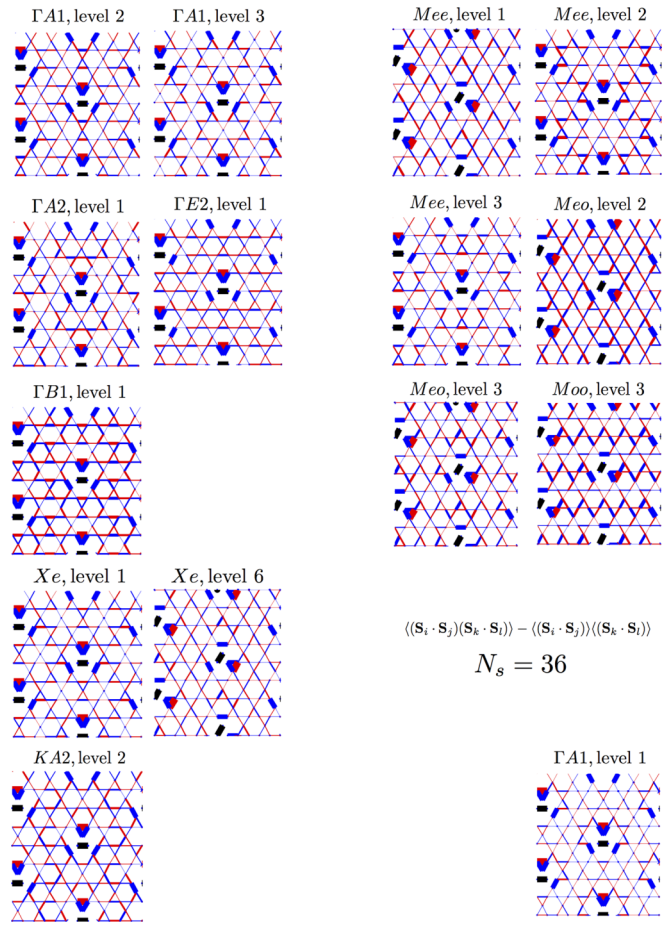

FIG. 5. Panel of $N_s = 36$ dimer-dimer singlet correlations (defined as indicated in the figure) in the states highlighted by orange circles in Fig. 1(b). For comparison we show the ground-state dimer-dimer correlations in the bottom right subplot.

[1] V. Elser, Nuclear Antiferromagnetism in a Registered ^{3}He Solid, Phys. Rev. Lett. **62**, 2405 (1989).

[2] C. Zeng and V. Elser, Numerical studies of antiferromagnetism on a kagomé net, Phys. Rev. B **42**, 8436 (1990).

[3] J. T. Chalker and J. F. G. Eastmond, Ground-state disorder in the spin-1/2 *kagomé* Heisenberg antiferromagnet, Phys. Rev. B **46**, 14201 (1992).

[4] P. W. Leung and V. Elser, Numerical studies of a 36-site *kagome* antiferromagnet, Phys. Rev. B **47**, 5459 (1993).

[5] P. Lecheminant, B. Bernu, C. Lhuillier, L. Pierre, and P. Sindzingre, Order versus disorder in the quantum heisenberg antiferromagnet on the *kagomé* lattice using exact spectra analysis, Phys. Rev. B **56**, 2521 (1997).

[6] Ch. Waldtmann, H.-U. Everts, B. Bernu, C. Lhuillier, P. Sindzingre, P. Lecheminant, and L. Pierre, First excitations of the spin 1/2 Heisenberg antiferromagnet on the kagome lattice, Eur. Phys. J. B **2**, 501 (1998).

[7] A. M. Läuchli, J. Sudan, and E. S. Sørensen, Ground-state energy and spin gap of spin-$\frac{1}{2}$ kagomé-Heisenberg antiferromagnetic clusters: Large-scale exact diagonalization results, Phys. Rev. B **83**, 212401 (2011).

[8] H. Nakano and T. Sakai, Numerical-diagonalization study of spin gap issue of the kagome lattice Heisenberg antiferromagnet, J. Phys. Soc. Jpn. **80**, 053704 (2011).

[9] H. J. Changlani, D. Kochkov, K. Kumar, B. K. Clark, and E. Fradkin, Macroscopically Degenerate Exactly Solvable Point in the Spin-1/2 Kagome Quantum Antiferromagnet, Phys. Rev. Lett. **120**, 117202 (2018).

[10] A. Wietek and A. M. Läuchli, Valence bond solid and possible deconfined quantum criticality in an extended kagome lattice Heisenberg antiferromagnet, arXiv:1908.02762 (2019).

[11] C. Zeng and V. Elser, Quantum dimer calculations on the spin-1/2 *kagome* Heisenberg antiferromagnet, Phys. Rev. B **51**, 8318 (1995).

[12] F. Mila, Low-Energy Sector of the $s = 1/2$ Kagome Antiferromagnet, Phys. Rev. Lett. **81**, 2356 (1998).

[13] M. Mambrini and F. Mila, RVB description of the low-energy singlets of the spin 1/2 kagomé antiferromagnet, Eur. Phys. J. B **17**, 651 (2000).

[14] G. Misguich, D. Serban, and V. Pasquier, Quantum Dimer Model on the Kagome Lattice: Solvable Dimer-Liquid and Ising Gauge Theory, Phys. Rev. Lett. **89**, 137202 (2002).

[15] G. Misguich, D. Serban, and V. Pasquier, Quantum dimer model with extensive ground-state entropy on the kagome lattice, Phys. Rev. B **67**, 214413 (2003).

[16] D. Poilblanc, M. Mambrini, and D. Schwandt, Effective quantum dimer model for the kagome Heisenberg antiferromagnet: Nearby quantum critical point and hidden degeneracy, Phys. Rev. B **81**, 180402(R) (2010).

[17] D. Schwandt, M. Mambrini, and D. Poilblanc, Generalized hard-core dimer model approach to low-energy Heisenberg frustrated antiferromagnets: General properties and application to the kagome antiferromagnet, Phys. Rev. B **81**, 214413 (2010).

[18] I. Rousochatzakis, Y. Wan, O. Tchernyshyov, and F. Mila, Quantum dimer model for the spin-$\frac{1}{2}$ kagome Z_2 spin liquid, Phys. Rev. B **90**, 100406(R) (2014).

[19] A. Ralko, F. Mila, and I. Rousochatzakis, Microscopic theory of the nearest-neighbor valence bond sector of the spin-$\frac{1}{2}$ kagome antiferromagnet, Phys. Rev. B **97**, 104401 (2018).

[20] Y. Ran, M. Hermele, P. A. Lee, and X.-G. Wen, Projected-Wave-Function Study of the Spin-1/2 Heisenberg Model on the Kagomé Lattice, Phys. Rev. Lett. **98**, 117205 (2007).

[21] Y. Iqbal, F. Becca, and D. Poilblanc, Projected wave function study of $\mathbb{Z}_2$ spin liquids on the kagome lattice for the spin-$\frac{1}{2}$ quantum Heisenberg antiferromagnet, Phys. Rev. B **84**, 020407(R) (2011).

[22] Y. Iqbal, F. Becca, and D. Poilblanc, Valence-bond crystal in the extended kagome spin-$\frac{1}{2}$ quantum Heisenberg antiferromagnet: A variational monte carlo approach, Phys. Rev. B **83**, 100404(R) (2011).

[23] T. Tay and O. I. Motrunich, Variational study of J_1-J_2 Heisenberg model on kagome lattice using projected Schwinger-boson wave functions, Phys. Rev. B **84**, 020404(R) (2011).

[24] B. K. Clark, J. M. Kinder, E. Neuscamman, Garnet Kin-Lic Chan, and M. J. Lawler, Striped Spin Liquid Crystal Ground State Instability of Kagome Antiferromagnets, Phys. Rev. Lett. **111**, 187205 (2013).

[25] Y. Iqbal, D. Poilblanc, and F. Becca, Vanishing spin gap in a competing spin-liquid phase in the kagome Heisenberg antiferromagnet, Phys. Rev. B **89**, 020407(R) (2014).

[26] O. Götze, D. J. J. Farnell, R. F. Bishop, P. H. Y. Li, and J. Richter, Heisenberg antiferromagnet on the kagome lattice with arbitrary spin: A higher-order coupled cluster treatment, Phys. Rev. B **84**, 224428 (2011).

[27] R. Budnik and A. Auerbach, Low-Energy Singlets in the Heisenberg Antiferromagnet on the Kagome Lattice, Phys. Rev. Lett. **93**, 187205 (2004).

[28] S. Capponi, A. Läuchli, and M. Mambrini, Numerical contractor renormalization method for quantum spin models, Phys. Rev. B **70**, 104424 (2004).

[29] S. Capponi, V. R. Chandra, A. Auerbach, and M. Weinstein, *p*6 chiral resonating valence bonds in the kagome antiferromagnet, Phys. Rev. B **87**, 161118(R) (2013).

[30] R. R. P. Singh and D. A. Huse, Three-Sublattice Order in Triangular- and Kagomé-Lattice Spin-Half Antiferromagnets, Phys. Rev. Lett. **68**, 1766 (1992).

[31] R. R. P. Singh and D. A. Huse, Ground state of the spin-1/2 kagome-lattice Heisenberg antiferromagnet, Phys. Rev. B **76**, 180407(R) (2007).

[32] H. C. Jiang, Z. Y. Weng, and D. N. Sheng, Density Matrix Renormalization Group Numerical Study of the Kagome Antiferromagnet, Phys. Rev. Lett. **101**, 117203 (2008).

[33] S. Yan, D. A. Huse, and S. R. White, Spin-liquid ground state of the s = 1/2 kagome Heisenberg antiferromagnet, Science **332**, 1173 (2011).

[34] S. Depenbrock, I. P. McCulloch, and U. Schollwöck, Nature of the Spin-Liquid Ground State of the $s = 1/2$ Heisenberg Model on the Kagome Lattice, Phys. Rev. Lett. **109**, 067201 (2012).

[35] H.-C. Jiang, Z. Wang, and L. Balents, Identifying topological order by entanglement entropy, Nat. Phys. **8**, 902 (2012).

[36] S. Nishimoto, N. Shibata, and C. Hotta, Controlling frustrated liquids and solids with an applied field in a kagome Heisenberg antiferromagnet, Nat. Commun. **4**, 2287 (2013).

[37] Y.-C. He, M. P. Zaletel, M. Oshikawa, and F. Pollmann, Signatures of Dirac Cones in a DMRG Study of the

Kagome Heisenberg Model, Phys. Rev. X **7**, 031020 (2017).

[38] G. Evenbly and G. Vidal, Frustrated Antiferromagnets with Entanglement Renormalization: Ground State of the Spin-$\frac{1}{2}$ Heisenberg Model on a Kagome Lattice, Phys. Rev. Lett. **104**, 187203 (2010).

[39] Z. Y. Xie, J. Chen, J. F. Yu, X. Kong, B. Normand, and T. Xiang, Tensor Renormalization of Quantum Many-Body Systems using Projected Entangled Simplex States, Phys. Rev. X **4**, 011025 (2014).

[40] J.-W. Mei, J.-Y. Chen, H. He, and X.-G. Wen, Gapped spin liquid with $\mathbb{Z}_2$ topological order for the kagome Heisenberg model, Phys. Rev. B **95**, 235107 (2017).

[41] S. Jiang, P. Kim, J. H. Han, and Y. Ran, Competing Spin Liquid Phases in the S=$\frac{1}{2}$ Heisenberg Model on the Kagome Lattice, SciPost Phys. **7**, 006 (2019).

[42] H. J. Liao, Z. Y. Xie, J. Chen, Z. Y. Liu, H. D. Xie, R. Z. Huang, B. Normand, and T. Xiang, Gapless Spin-Liquid Ground State in the $s = 1/2$ Kagome Antiferromagnet, Phys. Rev. Lett. **118**, 137202 (2017).

[43] The 36, 42, and 48 site clusters have, respectively, 54, 35, and 12 excess length-8 loops, i.e., loops which have a nontrivial winding number around the torus.

[44] A. M. Läuchli and R. Moessner, Quantum simulations made easy plane, arXiv:1504.04380 (2015).

[45] Y.-C. He and Y. Chen, Distinct Spin Liquids and their Transitions in Spin-1/2XXZ Kagome Antiferromagnets, Phys. Rev. Lett. **114**, 037201 (2015).

[46] We chose the 36*d* and 42*b* clusters in the notation of Ref. [7], while the 48 site cluster corresponds to a highly symmetric 4×4 unit-cell torus.

[47] M. Schuler, S. Whitsitt, L.-P. Henry, S. Sachdev, and A. M. Läuchli, Universal Signatures of Quantum Critical Points from Finite-Size Torus Spectra: A Window into the Operator Content of Higher-Dimensional Conformal Field Theories, Phys. Rev. Lett. **117**, 210401 (2016).

[48] B. Bauer, L. Cincio, B. P. Keller, M. Dolfi, G. Vidal, S. Trebst, and A. W. W. Ludwig, Chiral spin liquid and emergent anyons in a kagome lattice Mott insulator, Nat. Commun. **5**, 5137 (2014).

[49] Y.-C. He, D. N. Sheng, and Y. Chen, Chiral Spin Liquid in a Frustrated Anisotropic Kagome Heisenberg Model, Phys. Rev. Lett. **112**, 137202 (2014).

[50] S.-S. Gong, W. Zhu, and D. N. Sheng, Emergent chiral spin liquid: Fractional quantum hall effect in a kagome Heisenberg model, Sci. Rep. **4**, 6317 (2014).

[51] A. Wietek, A. Sterdyniak, and A. M. Läuchli, Nature of chiral spin liquids on the kagome lattice, Phys. Rev. B **92**, 125122 (2015).

[52] The precise sectors in the QDM are as follows: for $N_s = 36$ and 48, $3 \times \Gamma_{ee}$ and $1 \times \Gamma_{oe}$ (expressed as D_6 representations: $2 \times \Gamma_{A1}$ and $1 \times \Gamma_{E2}$); for $N_s = 42$, $2 \times \Gamma_e$ and $2 \times M_o$.

[53] In the variational calculation [25] the $S = 2$ gap was determined. Our $S = 1$ gap is about half as large as their $S = 2$ gap.

[54] M. Srednicki, Chaos and quantum thermalization, Phys. Rev. E **50**, 888 (1994).